Ultrasonics 102 (2020) 106032

Contents lists available at ScienceDirect

Ultrasonics

journal homepage: www.elsevier.com/locate/ultras

Influence of microstructural grain-size distribution on ultrasonic scattering

Musa Norouzian, Showmic Islam, Joseph A. Turner*

Department of Mechanical and Materials Engineering, W342 Nebraska Hall, University of Nebraska–Lincoln, Lincoln, NE 68588-0526, United States

A B S T R A C T

Ultrasonic attenuation and diffuse scattering result from the interaction of ultrasound with the microstructure of polycrystalline samples. Researchers are now using these effects to quantify mean grain size with good success and progress is being made with respect to more complex grain morphologies and macroscopic texture. However, theoretical models of such microstructures can become untenable because the scattering theory requires the two-point spatial statistics of the microstructure. For this reason, computational models of polycrystals are often considered for which grain spatial statistics can be calculated directly. In this study, the influence of grain-size distribution is examined using such an approach with three-dimensional (3D) realizations of polycrystalline materials. Representative material volumes are created using DREAM.3D with lognormal grain-size distributions, with fixed means but six different widths. These realizations are then used to calculate the relevant grain statistics which are then used to determine ultrasonic attenuation. The use of thirty realizations for each grain-size distribution allows the variation of the ultrasonic scattering to be quantified. The results show that the correlation between attenuation and distribution width can be modeled with a power law. Additionally, the frequency dependence of attenuation is shown to depend strongly on the distribution width. These results are expected to aid in the development of simplified models to quantify the grain-size distribution.

1. Introduction

In microscopic analysis of materials, a distribution of grain sizes is typically observed. Studies have shown that this grain-size distribution influences mechanical properties such as the flow stress [1,2], hardness [3,4], and yield stress [5,6]. Moreover,the corrosion behavior of materials is also influenced by the distribution. For instance, Gollapudi [7] found that in a non-passivating environment, corrosion resistance increases with the distribution width. In addition, mechanical properties such as material yield strength and ductility are greatly influenced by the grain size [8,9]. A recent study by Lin et al. [10] shows the possibility of achieving an optimum value between strength and ductility using graded microstructures. In fact, they found a distribution of coarse and nano grains for which both the ductility and strength surpass those of the purely coarse-grained material. These studies highlight the importance of grain size distribution to obtain high performance materials with tailored characteristics. Hence, quantification of these distributions is crucial.

Traditionally, the grain-size distribution in a material is obtained by linear intercept measurements from optical or scanning electron microscope (SEM) images [11]. Through electron backscatter diffraction (EBSD) images, microstructural information including grain size and orientation are obtained for a two-dimensional surface. In order to acquire more comprehensive information, serial sectioning techniques are used by which EBSD images are collected for several layers of the material [12,13]. These images are then reconstructed to form a digital three-dimensional (3D) representation of the material. Although these techniques provide extensive and valuable details, they are expensive, time consuming, and destructive. Studies [14–16] have shown that ultrasonic techniques can also be used for microstructural characterization. Unlike microscopy techniques, ultrasonic measurements are fast and non-destructive. A recent study by Dong et al. [17] shows the process of in-situ measurement of grain-size distribution using laser ultrasound. For accurate ultrasonic characterization, proper knowledge of ultrasonic responses in polycrystals is required.

Ultrasonic behavior in polycrystals has been studied extensively in the past. Mason and McSkimin [18] were the first to indicate that the acoustic impedance mismatch at grain boundaries is the main source of ultrasonic scattering and attenuation within polycrystalline materials. Later, Stanke and Kino [19] and Weaver [20] established two of the most prominent theoretical models correlating ultrasonic attenuation to microscopic and macroscopic properties of materials. However, both models typically consider only a single geometric length scale related to mean grain diameter. Several other assumptions are also included in those models [21]. A study by Smith [23] revealed the effect of grain-size distribution on ultrasonic attenuation. Using Roney's theory [22], he showed that materials with the same mean grain diameter but different distributions can have attenuations with significantly different frequency dependence. Later, Nicoletti and Anderson [24] presented a deconvolution method to study the inverse problem of finding the grain-size distribution from ultrasonic attenuation. In a recent study by Arguelles and Turner [25], an analytical attenuation form was proposed by assigning a volume fraction to each grain size in the effective spatial correlation function. Bai et al. [26] found that the theoretical

* Corresponding author.

https://doi.org/10.1016/j.ultras.2019.106032
Received 2 April 2019; Received in revised form 29 July 2019; Accepted 14 September 2019
Available online 17 September 2019
0041-624X/

expression in [25] agreed very well with their attenuation measurement of an α-titanium alloy. Similar to [25], Sha [27] provided an analytical formulation to correlate a volumetric grain size distribution to the ultrasonic attenuation. The results of [27] were shown to agree reasonably well with the finite element simulations of Ryzy et al. [28] which were based on Voronoi microstructures.

In this study, the effect of grain-size distribution on ultrasonic attenuation is investigated using a large number of synthetic 3D polycrystals created by DREAM.3D [29] which generates volumes based on a number distribution. Therefore, the mean and standard deviation of grain diameters are not weighted by their volumes. This description may be contrasted with the work of Arguelles and Turner [25] and Sha [27] that were based on a volume distribution. Here, all realizations have almost the same mean grain diameter but different distribution widths. To calculate the attenuation, the theoretical framework developed by Weaver [20] is used. However, unlike most previous studies, no assumptions are considered regarding the morphological and orientational properties. As such, the attenuation values are calculated directly from the synthetic volumes. In Section 2, the computational framework is discussed and the conventional assumptions are outlined. Section 3 provides the details of the material properties and the statistics of the 180 synthetic realizations. A discussion of the results is presented in Section 4, including the examination of the two-point statistics and the frequency dependence of the attenuation.

2. Computational framework

Using ensembles of synthetic volumes, the influence of grain-size distribution width on ultrasonic attenuation can be investigated. Norouzian and Turner [21] introduced the methodology to obtain the attenuation values using synthetic microstructures. In that work, the theoretical framework developed by Weaver [20] was modified to handle the discrete nature of these microstructures. For completeness, an overview of the technique is included here.

2.1. Attenuation of discrete microstructures

For an incident wave propagating in the $\hat{\mathbf{p}}$ direction with polarization direction $\hat{\mathbf{u}}$ that scatters into direction with polarization direction $\hat{\mathbf{v}}$, the scattering coefficient can be defined as

$$\Omega^{\hat{\mathbf{u}}\to\hat{\mathbf{v}}}(\hat{\mathbf{p}},\,\hat{\mathbf{s}}) = \frac{\omega^4}{32\pi^2\rho^2\left[C_I^{\hat{\mathbf{u}}}(\hat{\mathbf{p}})\right]^3\left[C_S^{\hat{\mathbf{v}}}(\hat{\mathbf{s}})\right]^5}\int \mathbf{\Lambda}(\mathbf{r})^{\cdots\hat{\mathbf{u}}\hat{\mathbf{p}}\hat{\mathbf{s}}\hat{\mathbf{v}}}_{\cdots\hat{\mathbf{u}}\hat{\mathbf{p}}\hat{\mathbf{s}}\hat{\mathbf{v}}}\, e^{-i\left[\frac{\omega}{C_I^{\hat{\mathbf{u}}}}\hat{\mathbf{p}}-\frac{\omega}{C_S^{\hat{\mathbf{v}}}}\hat{\mathbf{s}}\right].\mathbf{r}}\,\mathrm{d}\mathbf{r}, \tag{1}$$

where ω is the frequency, ρ is material density and $\mathbf{r} = \mathbf{x} - \mathbf{x}'$ is the separation vector between two positions $\mathbf{x}$ and $\mathbf{x}'$. $C_I^{\hat{\mathbf{u}}}$ and $C_S^{\hat{\mathbf{v}}}$ define the phase velocity of the incident wave polarized in the $\hat{\mathbf{u}}$ direction and the phase velocity of the scattered wave polarized in the $\hat{\mathbf{v}}$ direction, respectively. $\mathbf{\Lambda}$ is the covariance function of the elastic modulus $\mathbf{C}$ in which information regarding the spatial distribution of material heterogeneity is defined. The inner product between the covariance function and the propagation and polarization vectors included in Eq. (1) is given in direct notation by

$$\mathbf{\Lambda}(\mathbf{r})^{\cdots\hat{\mathbf{u}}\hat{\mathbf{p}}\hat{\mathbf{s}}\hat{\mathbf{v}}}_{\cdots\hat{\mathbf{u}}\hat{\mathbf{p}}\hat{\mathbf{s}}\hat{\mathbf{v}}} = \langle \delta C_{ijkl}(\mathbf{x})\,\delta C_{\alpha\beta\gamma\delta}(\mathbf{x}+\mathbf{r})\rangle \hat{u}_i\hat{u}_\alpha\hat{p}_j\hat{p}_\beta\hat{s}_k\hat{s}_\gamma\hat{v}_l\hat{v}_\delta, \tag{2}$$

where $\delta\mathbf{C}$ is the modulus fluctuation about the mean. Because the material information is known at discrete locations, a discrete form of Eq. (1) may be defined. This integration is achieved using a Monte Carlo scheme. Hence, Eq. (1) can be rewritten as

$$\Omega^{\hat{\mathbf{u}}_j\to\hat{\mathbf{v}}_k}(\hat{\mathbf{p}},\,\hat{\mathbf{s}}) = \frac{R^3\omega^4}{24\pi\rho^2 NN_p\left[C_I^{\hat{\mathbf{u}}_j}(\hat{\mathbf{p}})\right]^3\left[C_S^{\hat{\mathbf{v}}_k}(\hat{\mathbf{s}})\right]^5} \times\sum_{n=1}^{N}\left[\sum_{m=1}^{N_p}\delta\mathbf{C}(\mathbf{x}_m)\,\delta\mathbf{C}(\mathbf{x}_m+\mathbf{r}_n)\right]^{\cdots\hat{\mathbf{u}}_j\hat{\mathbf{p}}\hat{\mathbf{s}}\hat{\mathbf{v}}_k}_{\cdots\hat{\mathbf{u}}_j\hat{\mathbf{p}}\hat{\mathbf{s}}\hat{\mathbf{v}}_k} e^{-i\mathbf{q}\cdot\mathbf{r}_n}, \tag{3}$$

where $\mathbf{x}$ is a randomly selected location in the volume, N_p is the total number of locations, N is the number of discrete points used for the integration, and R is the largest distance used to calculate the two-point statistics. As discussed in [21], when modeling microstructures with equiaxed grains and weak texture, R should be given a value close to the largest grain diameter of the volume in order to achieve convergence. This conjecture is based on the fact that two-point correlations become almost negligible at distances larger than the maximum grain diameter [21]. The vector $\mathbf{q}$ in Eq. (3) is defined as $\mathbf{q} = \frac{\omega}{C_I^{\hat{\mathbf{u}}_j}}\hat{\mathbf{p}} - \frac{\omega}{C_S^{\hat{\mathbf{v}}_k}}\hat{\mathbf{s}}$ and in spherical coordinates, $\mathbf{r}_n$ is given as

$$\mathbf{r}_n = r_n[\sqrt{1-\mu_n^2}\cos(\phi_n) + \sqrt{1-\mu_n^2}\sin(\phi_n) + \mu_n], \tag{4}$$

where $\mu = \cos(\theta)$. Here, r, μ and ϕ are obtained using a random variable set $\boldsymbol{\lambda} \in [0,\,1]^3$. To ensure uniform sampling of the integration volume, they are defined by

$$r = R\lambda_1^{1/3}, \quad \mu = 2\lambda_2 - 1, \quad \phi = 2\pi\lambda_3. \tag{5}$$

where λ_i belongs to the set $\boldsymbol{\lambda}$. Attenuation is defined as the integral of the scattering coefficient over all scattering directions. This integration is performed in the same manner as that for the scattering coefficient. The number of scattering directions required to achieve convergence depends upon the degree of statistical anisotropy of the microstructure. For materials with absolute isotropy, only a single direction is sufficient for accurate calculation. However, the number of required directions increases with statistical anisotropy.

2.2. Decoupling of the covariance function

In most ultrasonic theories, the covariance function is decoupled into tensorial and spatial components [19,20,25,27]. This assumption helps with the analytical formulation of the covariance function and hence, the scattering coefficient. The validity of this assumption was established in Ref. [21] for microstructures with a narrow grain size distribution. However, for wider distributions, similar studies are required. Considering the decoupling assumption, Eq. (3) can be rewritten as

$$\Omega^{\hat{\mathbf{u}}_j\to\hat{\mathbf{v}}_k}(\hat{\mathbf{p}},\,\hat{\mathbf{s}}) = \frac{R^3\omega^4}{24\pi\rho^2 VNN_pN_g\left[C_I^{\hat{\mathbf{u}}_j}(\hat{\mathbf{p}})\right]^3\left[C_S^{\hat{\mathbf{v}}_k}(\hat{\mathbf{s}})\right]^5} \times\sum_{n=1}^{N}\left[\sum_{m=1}^{N_p}\sum_{l=1}^{N_g}\delta\mathbf{C}_l^2 V_l I(\mathbf{x}_m,\,\mathbf{x}_m+\mathbf{r}_n)\right]^{\cdots\hat{\mathbf{u}}_j\hat{\mathbf{p}}\hat{\mathbf{s}}\hat{\mathbf{v}}_k}_{\cdots\hat{\mathbf{u}}_j\hat{\mathbf{p}}\hat{\mathbf{s}}\hat{\mathbf{v}}_k} e^{-i\mathbf{q}\cdot\mathbf{r}_n}, \tag{6}$$

where N_g is the total number of grains, V is the volume of the synthetic microstructure, and $\delta\mathbf{C}_l$ and V_l are the modulus fluctuation and volume of the l^{th} grain, respectively. The indicator $I(\mathbf{x},\,\mathbf{x}')$ is defined as unity if $\mathbf{x}$ and $\mathbf{x}' = \mathbf{x} + \mathbf{r}$ are located within the same grain, and zero otherwise. The derivation details of Eqs. (3) and (6) can be found in Ref. [21]. It should be noted that the use of the decoupling assumption not only simplifies the analytical formulation of the problem, but also reduces the computation time. This efficiency is in essence due to the tensorial character of the modulus fluctuation versus the scalar form of the indicator I.

3. Synthetic volume generation

In this work, the influence of distribution width on the ultrasonic responses is investigated. This goal is attained by using synthetic volumes with fixed mean grain diameter but different distribution widths

generated by DREAM.3D [29]. All microstructures are assumed to be made of nickel with single crystal elastic properties of $c_{11} = 247$, $c_{12} = 153$, and $c_{44} = 122$ GPa [30] and density of $\rho = 8900$ kg/m^3. Considering a mean grain diameter of $D = 30$ μm with six standard deviations covering a range from 3 μm to 18 μm, a group of 180 microstructures are created (30 realizations in each ensemble). These microstructures have a volume of 1200^3 μm^3 and contain grains of cubic symmetry. The grain sizes have a log-normal distribution, $f(d)$, defined as

$$f(d) = \frac{1}{d\sigma\sqrt{2\pi}}\, e^{-\frac{(\ln d-\mu)^2}{2\sigma^2}}, \tag{7}$$

where d is the grain diameter, and μ and σ are the average and standard deviation (SD) of grain diameter in log-space, respectively. The log-space statistics are required by DREAM.3D to generate the realizations. The focus of this study is to understand the influence of distribution width on ultrasonic responses. Therefore, it is crucial to have microstructures with nearly the same mean grain diameter. Creating these microstructures proved to be challenging because the grain-size statistics obtained from the software often deviate from the desired ones, especially for wide distributions. Hence, the input parameters μ and σ are modified in order to correct the deviation. Table 1 provides the input parameters for desired grain size statistics along with the obtained statistics across the ensemble of synthetic microstructures. The obtained grain diameters given in Table 1 shows that the six ensembles of volumes have very a similar mean. The maximum diameter represents the average of the largest grain diameters across the ensemble. Moreover, Table 1 shows that for a constant volume, wider grain-size distributions contain a smaller number of grains. This property is expected due to the presence of larger grains in those wider distributions.

Previously [21], it was shown that the grain-size statistics of the boundary grains are not similar to the interior ones. Specifically, the exterior grains are statistically larger than the interior ones. Therefore, the authors suggested that studies should be conducted on a smaller section of the volume that is selected from the interior to ensure a spatially homogeneous distribution. Here, a similar approach is taken with all volumes sectioned according to their grain-size distribution. Each sectioned volume is selected from the center of the 1200^3 μm^3 volume such that each face is closer to the center by an amount three times the standard deviation of the grain size, Σ. Hence, each dimension of the final volume is $l = (1200 - 6\Sigma)$ μm. The grain statistics of the new volumes are given in Table 2. Comparison of the statistics given in Tables 1 and 2, the mean grain diameter decreases after the sectioning process. This decrease indicates that relatively larger grains reside on the 6 faces. Such an observation agrees with [21].

To provide a better understanding of the synthetic volumes, an example microstructure of each distribution is illustrated in Fig. 1. These microstructures represent the volumes after sectioning. For wider distributions, curved grain boundaries are clearly visible. Such boundaries - also observed in real microstructures - are the distinct difference between Voronoi tessellations and DREAM.3D volumes. In addition, it is known that Voronoi tessellations have limitations when attempting to create wide distributions [31,32]. However, Fig. 1 exhibits the capability of DREAM.3D for such microstructures.

4. Results and discussion

The integration required to calculate the attenuation for each synthetic volume is based on a total of 1000 scattering directions. For each direction, the scattering coefficient is calculated using $N = 5000$ discrete points. For the simulated nickel microstructure, the quasi-longitudinal and quasi-shear attenuations are calculated for a 15 MHz wave propagating in the [0 0 1] direction. These attenuation results are given in Table 3.

The influence of distribution width is clearly shown in Table 3. Although the mean grain diameter of all blocks is very similar, larger grain-size distributions result in much higher attenuation values. This phenomenon is primarily due to the higher scattering from the larger grains. Because the volume fraction of large grains is higher in wider distributions, higher attenuations are observed. Theories based on a single material length scale are unable to capture such differences. For instance, using exponential two-point statistics and Voigt averaging, the longitudinal and shear attenuations of a nickel microstructure with a 29.4 μm mean grain diameter are 22.75 and 89.41 Np/m, respectively. These predictions are independent of the distribution width.

The attenuation results also exhibit a slight anisotropy. For microstructures with absolute isotropy, the two modes of shear attenuation would be identical. However, the results here show up to a 3 percent difference in the shear attenuations. Such anisotropy is likely related to two factors. The first one is the influence of the finite number of grains comprising the microstructures. It was observed by Norouzian and Turner [33] that the degree of statistical isotropy increases with the number of grains for polycrystals with randomly oriented grains. Hence, higher statistical isotropy is expected for narrow distributions due to their larger number of grains. In addition, the Euler angles of volumes created by DREAM.3D have been observed to deviate slightly from a purely random orientation [33]. Both of these factors play a role in the attenuation anisotropy shown here.

4.1. Assumptions of the two-point statistics

Typically, the two-point spatial correlation function is expressed as an exponential function using a correlation length which corresponds with the mean grain radius [19,20]. Such a theoretical function is defined as $\eta(r) = \exp(-r/L)$, where L is the spatial correlation length. Hence, two microstructures that have identical mean grain diameter, but different standard deviations show similar two-point statistics. The validity of such a theoretical assumption is exhibited in Fig. 2. This figure shows the two-point spatial correlation function for the six microstructures with nearly identical mean grain diameter but different

Table 1
Microstructural information of the 6 different ensembles created using the input statistics given in the log-space. The output values are the average of the 30 realizations in each ensemble. D and Σ are the mean and standard deviation of the grain diameters in the linear-space, respectively. In addition, Maximum Diameter represents the average diameter of the largest grain in each ensemble. The variation of each parameter is obtained using all realizations belonging to an ensemble. Finally, the parameter Number of Grains shows the effect of grain-size distribution on the total number of grains comprising the volumes.

Ensemble No.	Input Statistics		Output Statistics		Maximum Diameter (μm)	Number of Grains
	μ	σ	D (μm)	Σ (μm)		
1	3.3962	0.0998	29.6 ± 0.0	3.6 ± 0.2	45.1 ± 0.6	122198 ± 72
2	3.3816	0.1980	29.8 ± 0.0	5.7 ± 0.4	56.0 ± 0.9	112475 ± 136
3	3.327	0.3853	30.5 ± 0.0	10.3 ± 0.5	88.2 ± 0.8	83213 ± 69
4	3.25	0.5	30.4 ± 0.1	13.0 ± 1.0	114.5 ± 1.4	69042 ± 402
5	3.1	0.6654	30.5 ± 0.1	16.4 ± 1.7	159.9 ± 2.5	50070 ± 739
6	2.92	0.78	29.7 ± 0.2	17.9 ± 2.4	186.9 ± 2.9	44082 ± 1113

Table 2
Grain statistics of the volumes obtained after sectioning. For each distribution, D and Σ are the mean and the standard deviation of grain diameters obtained using the volumes of the new ensembles. From this point forward, all calculations are performed using the sectioned microstructures.

Ensemble No.	D (μm)	Σ (μm)	Σ/D	Maximum Diameter (μm)	Number of Grains
1	28.8 ± 0.0	6.6 ± 0.7	0.229 ± 0.001	44.9 ± 0.6	122107 ± 74
2	29.0 ± 0.0	10.5 ± 1.3	0.364 ± 0.003	56.0 ± 0.9	110327 ± 157
3	29.7 ± 0.0	13.6 ± 1.6	0.459 ± 0.003	88.0 ± 0.8	75435 ± 96
4	29.7 ± 0.1	15.5 ± 1.8	0.522 ± 0.004	114.1 ± 1.6	59666 ± 379
5	29.9 ± 0.1	18.3 ± 2.3	0.614 ± 0.003	159.3 ± 2.8	40604 ± 696
6	29.1 ± 0.2	19.4 ± 2.8	0.666 ± 0.004	186.2 ± 3.2	34554 ± 1001

distribution width. Analogous to the attenuation results in Table 3, the influence of distribution on spatial correlation function is evident. Wider distributions clearly show longer correlation lengths. In Fig. 2, the exponential dashed line defines the statistics often used in several previous studies [34–38]. It is interesting that the theory is closest to the grain distribution with standard deviation of about 13 μm. Assuming that the decoupling of the covariance function is valid, it is expected that the theoretical attenuation obtained assuming an exponential two-point correlation function is closest to the values of such a grain-size distribution.

In order to assess the validity of the decoupling assumption, the attenuation values must be calculated using the decoupled form of the scattering coefficient given in Eq. (6). In this case, the tensorial component of the covariance function is decoupled from the spatial part. Fig. 3 shows the attenuation values with and without the decoupling assumption for a 15 MHz wave propagating in the [0 0 1] direction. The results show a clear agreement between the two approaches. Attenuations calculated using the direct method show higher uncertainty bounds compared with their decoupled counterparts. This difference originates in part from the sufficiency of the statistics used to calculate the covariance function. For the direct method, the variations are primarily the result of the number of grains, but the decoupled method is governed by the number of voxels.

Moreover, the attenuation as a function of distribution width given in Table 3 can be fit with a power-law of the form $\alpha = a + b(\Sigma/D)^n$. Table 4 gives the fit parameters for the three modes of attenuation. The values provided in this table apply only to microstructures with an approximate mean grain diameter of 30 μm and incident wave with 15 MHz frequency. It is interesting that the attenuation scales with the ratio of the standard deviation and mean grain diameter with a power of around 4–4.5. It is unclear at this time if such a trend is also valid for other microstructures and frequency ranges.

Table 3
Attenuations (Np/m) calculated using the direct method for the six distributions. α_{qL} is the quasi-longitudinal attenuation, and α_{qT1} and α_{qT2} are the two modes of quasi-shear attenuation.

Σ (μm)	Σ/D	α_{qL}	α_{qT1}	α_{qT2}
6.6	0.229	6.10 ± 0.03	29.5 ± 0.20	29.54 ± 0.19
10.5	0.364	7.93 ± 0.07	38.02 ± 0.31	37.82 ± 0.37
13.6	0.459	18.77 ± 0.33	85.30 ± 0.99	84.98 ± 1.06
15.5	0.522	33.17 ± 0.83	141.49 ± 2.27	141.10 ± 2.76
18.3	0.614	67.63 ± 2.40	265.36 ± 8.45	263.45 ± 7.35
19.4	0.666	93.46 ± 2.84	359.81 ± 13.06	348.96 ± 13.02

In addition, the horizontal dashed line in Fig. 3 represents the attenuation for a Voigt-average medium with a correlation length of $L = 14.7$ μm. This correlation length represents the average grain radius of all synthetic volumes. For a standard deviation of 13.6 μm (about 0.46 times the mean diameter), the attenuation values of synthetic volumes are closest to the Voigt-average medium with exponential two-point statistics. The results show that for the lowest standard deviation, the quasi-longitudinal attenuation is about 3.7 times smaller than the attenuation calculated using exponential two-point statistics. On the other hand, for the widest distribution, this attenuation is 4.1 times larger than the results based on exponential two-point statistics. Finally, in Section 2.2, it was noted that the computational cost depends strongly on the decoupling assumption. For the results presented here, the decoupled attenuations are obtained approximately 90 times faster than those calculated using the direct formulation.

4.2. Frequency dependence of attenuation

The dependence of the attenuation on frequency is important if

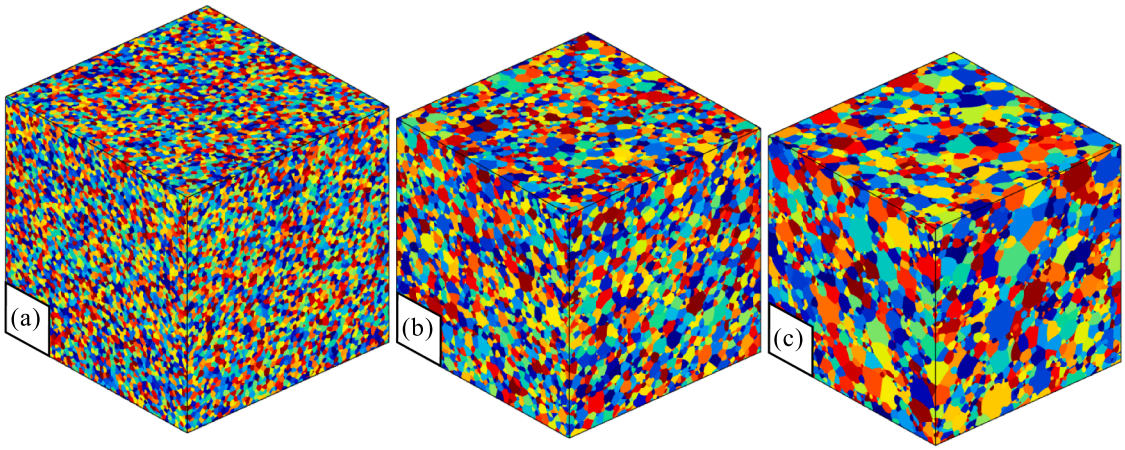

Fig. 1. Example microstructures from 3 grain-size distributions obtained after sectioning. The grain size statistics of these microstructures are: (a) $D = 28.8$ μm, $\Sigma = 6.5$ μm, (b) $D = 29.7$ μm, $\Sigma = 15.3$ μm, (c) $D = 29.0$ μm, $\Sigma = 19.3$ μm. The relative dimensions are conserved in (a), (b), and (c). Similar statistics across the ensemble are given in Table 2. It should be noted that the colors do not represent the orientation of grains but are used to identify individual grains. (For interpretation of the references to colour in this figure caption, the reader is referred to the web version of this article.)

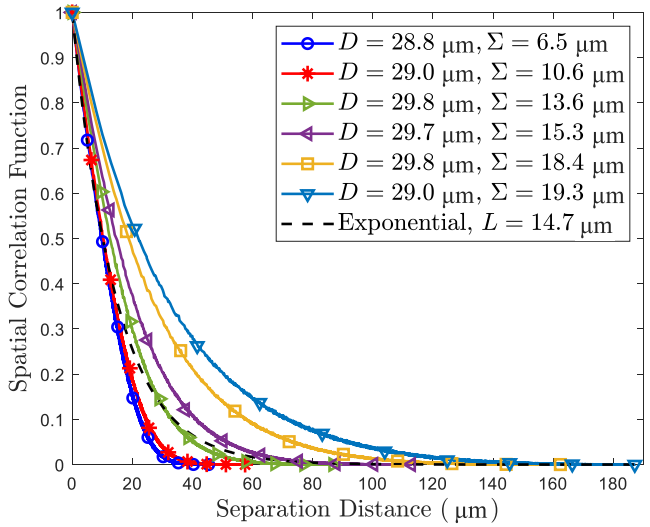

Fig. 2. Two-point spatial correlation function of synthetic microstructures with different grain size statistics along with an exponential form using spatial correlation length of $L = 14.7\,\mu m$. This correlation length represent the average grain radius of all the synthetic volumes.

attenuation measurements are to be used for microstructure characterization. For a practical frequency range, the attenuation has been observed to scale with frequency to a power ranging from 1.5 to 3.5 [41]. A similar range has been reported in other empirical studies [40,42,43]. Typically, in laser ultrasonics, a cubic frequency dependence is used to interpret changes in grain size during heat treatment [16,41,44]. These observations are within the theoretical limits. For instance, the low-frequency, theoretical dependence of attenuation, defined as Rayleigh scattering, has a dependence on frequency to the fourth power. At higher frequencies, for which the wavelength is comparable with the grain diameter, the attenuation scales with the second power of frequency (the stochastic scattering regime [39]). Here, the dependence with respect to frequency is examined for the synthetic volumes generated. To understand the results, it is necessary to quantify the wavelength for comparison with the mean grain diameter. The wavelength is found using phase velocity information as described previously [33]. The average quasi-longitudinal and two modes of quasi-shear velocities across the ensemble are given in Table 5. It is important to note that these results do not consider dispersion effects from scattering. The table clearly shows that both the uncertainty and statistical anisotropy increase as a function of the distribution width. This effect is primarily due to the smaller number of grains present in the wider distributions. A more comprehensive discussion of this behavior can be found in [33].

Table 4
Fitting parameters relating attenuation to distribution width using a power-law of the form $\alpha = a + b(\Sigma/D)^n$. It should be noted that these fit parameters apply only to the examples here (15 MHz frequency and volumes with average grain diameter of about 30 μm). α_{qL} is the quasi-longitudinal attenuation, and α_{qT1} and α_{qT2} are the two modes of quasi-shear attenuation.

Fit Parameters	α_{qL}	α_{qT1}	α_{qT2}
a [Np/m]	3.73	19.51	18.33
b [Np/m]	582.6	1946	1797
n	4.58	4.27	4.14

Table 5
The statistics of phase velocities across the ensembles for the six distributions. The standard deviation is used to represent the uncertainties. C_{qL}, C_{qT1}, and C_{qT2} (in m/s) are the quasi-longitudinal and the two modes of quasi-shear phase velocities, respectively.

Σ (μm)	C_{qL}	C_{qT1}	C_{qT2}
6.6	5903.8 ± 0.7	3186.4 ± 0.7	3187.5 ± 0.9
10.5	5904.0 ± 0.9	3186.1 ± 1.1	3187.6 ± 1.0
13.6	5904.4 ± 1.5	3185.2 ± 1.6	3187.6 ± 1.7
15.5	5903.9 ± 2.1	3185.6 ± 2.4	3188.2 ± 2.2
18.3	5903.4 ± 3.4	3184.6 ± 4.0	3190.1 ± 3.5
19.4	5903.1 ± 5.3	3182.7 ± 5.6	3192.5 ± 5.9

Using Table 5, the longitudinal and shear wavelengths for a 15 MHz wave in a nickel polycrystal are found to be 393.6 μm and 212.5 μm, respectively. Hence, at this frequency, the maximum grain diameters are always smaller than the smallest wavelength for all distributions. Additionally, for the narrowest distribution in which the maximum grain diameter is 45 μm, the scattering from all grains is within the Rayleigh limit. This scattering regime is expected because the smallest wavelength is 4.7 times larger than the largest grain diameter for this narrowest distribution. However, by increasing the distribution width, the volume fraction of large grains increases and consequently, the scattering regime is expected to transition towards the stochastic. This behavior is clearly seen in Fig. 4 in which the attenuation values are shown as a function of frequency for all six distributions. Note that for each distribution, only a single realization is used because the variation is negligible on this log-log scale. In this figure, the quasi-shear attenuation at 15 MHz for the smallest distribution scales with frequency to the power of 3.86 and drops to 2.45 for the widest distribution.

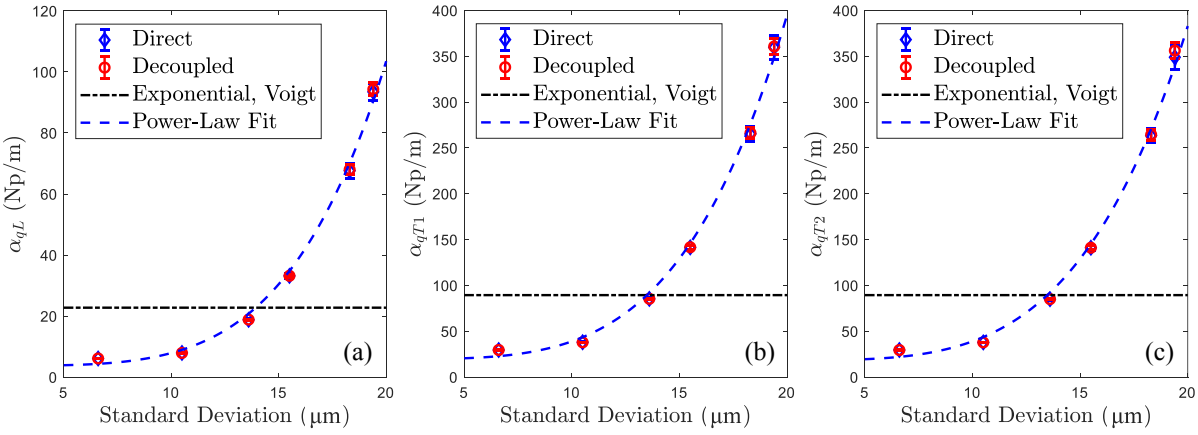

Fig. 3. Attenuations calculated using direct and decoupled methods for a 15 MHz wave as a function of the distribution width, (a) quasi-longitudinal, (b) first quasi-shear, and (c) second quasi-shear attenuations. The dashed line represents the value obtained using Voigt averaging method. Exponential spatial correlation functions use a correlation length of $L = 14.7\,\mu m$.

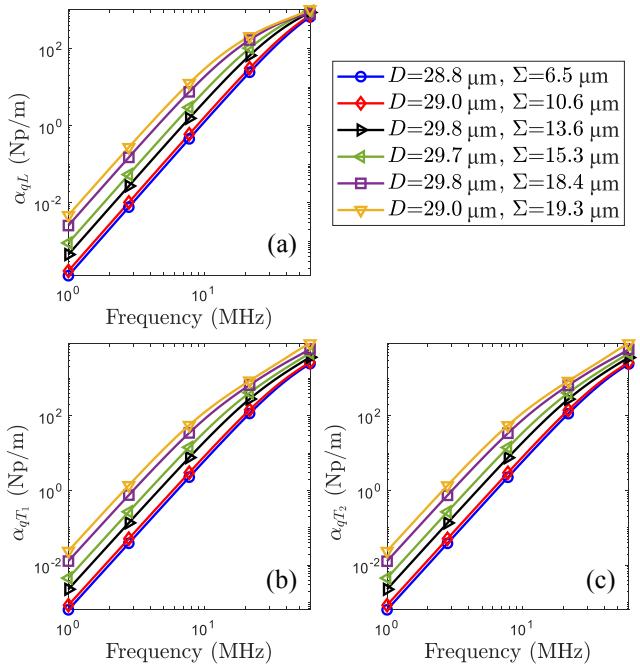

Fig. 4. Attenuation as a function of frequency for the 6 distributions. For each distribution, only one realization is used.

Table 6
Frequencies (MHz) at which the quasi-longitudinal and quasi-shear attenuations scale with the third power of frequency. The quasi-shear values are valid for both α_{qT1} and α_{qT2}.

Σ (μm)	quasi-Longitudinal	quasi-shear
6.6	43.1	35.0
10.5	37.3	32.4
13.6	25.6	20.8
15.5	19.4	15.7
18.3	12.7	11.1
19.4	10.6	8.6

Moreover, Fig. 4 shows that the frequency at which the Rayleigh scattering transitions to stochastic is a function of the distribution width. This property can be quantified more explicitly by considering the transition frequency to be that for which the attenuation scales with its third power. Table 6 provides such frequencies for the results shown in Fig. 4. This table shows that for the narrowest standard deviation, the transition occurs at a frequency 4 times larger than that of the widest distribution. Similar observations were made regarding the transition point for the approach of Arguelles and Turner [25]. In their work, the effective spatial correlation function was obtained by assigning a volume fraction to each grain size. Such a function was then used within Weaver's model [20] to achieve a semi-analytical form for the attenuation. For instance, for low frequencies, they found the slope of the attenuation curve decreased by about 18 percent when the distribution width was quadrupled. In addition, in the low frequency regime of Fig. 4, the attenuation scales with the fourth power of frequency for all distribution widths. However, at high frequencies the slope decreases to 2.3 for the narrowest distribution and drops to around 1.5 for the wider ones. These results agree well with the empirical values discussed by Sarkar [41].

5. Summary

The influence of grain size distribution on the ultrasonic attenuation has been studied using synthetic nickel microstructures simulated with DREAM.3D. These 180 realizations have a mean grain diameter of about 30 μm and standard deviation ranging from 3 μm to 18 μm. To eliminate the influence of the boundary grains, all volumes were sectioned according to their distribution width. These sectioned volumes were ultimately used to calculate the attenuation.

To obtain attenuation, a modified version of Weaver's model was used due to the discrete nature of material information. For a 15 MHz wave, the attenuation was found to increase with distribution width. In addition, for wider distributions, longer correlation length was observed in the spatial correlation functions. This behavior is due to the presence of larger grains for those distributions. Using these geometric spatial correlation function, attenuation values were obtained under the assumption of decoupling. This assumption was validated by comparing the direct and decoupled attenuations. The validity of decoupling is a proof that the correlation between attenuation and distribution width is related to the grain morphology and not orientation. It should be emphasized that such an argument is only valid if decoupling is valid. Also, using a power-law, the correlation between the attenuation and distribution width was quantified. Moreover, the attenuations for different distributions as a function of frequency showed that the transition from the Rayleigh to the stochastic regime occurs at lower frequencies for wider distributions. However, a detailed comparison with previous findings requires a resolution regarding differences between the number distribution approach and the volume distribution approach. The results of this article clearly show the importance of the distribution width in modeling the ultrasonic responses. Most classical models referenced in this article account for only the mean grain size and are not able to capture the influence of the distribution width. Hence, modifications must be made to those models in order to include the role of the distribution width more comprehensively. Such a modification is crucial for accurate microstructure characterization.

Acknowledgments

This work was supported by the Air Force Research Laboratory under prime contract FA8650-15-D-5231 and was completed utilizing the Holland Computing Center of the University of Nebraska, which receives support from the Nebraska Research Initiative.

Appendix A. Supplementary material

Supplementary data associated with this article can be found, in the online version, at https://doi.org/10.1016/j.ultras.2019.106032.

References

[1] S. Berbenni, V. Favier, M. Berveiller, Micro-macro modelling of the effects of the grain size distribution on the plastic flow stress of heterogeneous materials, Comput. Mater. Sci. 39 (1) (2007) 96–105.
[2] J.J. Bucki, K.J. Kurzydowski, Analysis of the effect of grain size uniformity on the flow stress of polycrystals: part ii: application of the studies to the flow stress of aluminium, Mater. Charact. 29 (3) (1992) 375–380.
[3] O. El-Atwani, D.V. Quach, M. Efe, P.R. Cantwell, B. Heim, B. Schultz, E.A. Stach, J.R. Groza, J.P. Allain, Multimodal grain size distribution and high hardness in fine grained tungsten fabricated by spark plasma sintering, Mater. Sci. Eng. A 528 (18) (2011) 5670–5677.
[4] E. Hall, Variation of hardness of metals with grain size, Nature 173 (4411) (1954) 948.
[5] S. Berbenni, V. Favier, M. Berveiller, Impact of the grain size distribution on the yield stress of heterogeneous materials, Int. J. Plast. 23 (1) (2007) 114–142.
[6] N. Hansen, Hall–Petch relation and boundary strengthening, Scripta Mater. 51 (8) (2004) 801–806.
[7] S. Gollapudi, Grain size distribution effects on the corrosion behaviour of materials, Corros. Sci. 62 (2012) 90–94.
[8] V. Imayev, R. Imayev, G. Salishchev, M. Shagiev, A. Kuznetsov, K. Povarova, Effect of strain rate on twinning and room temperature ductility of TiAl with fine equiaxed microstructure, Scripta Mater. 36 (8) (1997).
[9] R. Imayev, N. Gabdullin, G. Salishchev, O. Senkov, V. Imayev, F. Froes, Effect of grain size and partial disordering on ductility of Ti3Al in the temperature range of 20–600 °C, Acta Mater. 47 (6) (1999) 1809–1821.
[10] Y. Lin, J. Pan, H. Zhou, H. Gao, Y. Li, Mechanical properties and optimal grain size

distribution profile of gradient grained nickel, Acta Mater. 153 (2018) 279–289.
[11] K. Mingard, B. Roebuck, E. Bennett, M. Gee, H. Nordenstrom, G. Sweetman, P. Chan, Comparison of ebsd and conventional methods of grain size measurement of hardmetals, Int. J. Refract. Met. Hard Mater. 27 (2) (2009) 213–223.
[12] M.A. Groeber, B. Haley, M.D. Uchic, D.M. Dimiduk, S. Ghosh, 3D reconstruction and characterization of polycrystalline microstructures using a FIB–SEM system, Mater. Charact. 57 (4–5) (2006) 259–273.
[13] M.D. Uchic, M.A. Groeber, D.M. Dimiduk, J. Simmons, 3D microstructural characterization of nickel superalloys via serial-sectioning using a dual beam fib-sem, Scripta Mater. 55 (1) (2006) 23–28.
[14] R.B. Thompson, F. Margetan, P. Haldipur, L. Yu, A. Li, P. Panetta, H. Wasan, Scattering of elastic waves in simple and complex polycrystals, Wave Motion 45 (5) (2008) 655–674.
[15] C.M. Kube, Attenuation of laser generated ultrasound in steel at high temperatures; comparison of theory and experimental measurements, Ultrasonics 70 (2016) 238–240.
[16] M. Keyvani, T. Garcin, D. Fabrègue, M. Militzer, K. Yamanaka, A. Chiba, Continuous measurements of recrystallization and grain growth in cobalt super alloys, Metall. Mater. Trans. A 48 (5) (2017) 2363–2374.
[17] F. Dong, X. Wang, Q. Yang, H. Liu, D. Xu, Y. Sun, Y. Zhang, R. Xue, S. Krishnaswamy, In-situ measurement of Ti-6Al-4V grain size distribution using laser-ultrasonic technique, Scripta Mater. 154 (2018) 40–44.
[18] W. Mason, H. McSkimin, Attenuation and scattering of high frequency sound waves in metals and glasses, J. Acoust. Soc. Am. 19 (3) (1947) 464–473.
[19] F.E. Stanke, G.S. Kino, A unified theory for elastic wave propagation in polycrystalline materials, J. Acoust. Soc. Am. 75 (3) (1984) 665–681.
[20] R.L. Weaver, Diffusivity of ultrasound in polycrystals, J. Mech. Phys. Solids 38 (1) (1990) 55–86.
[21] M. Norouzian, J.A. Turner, Ultrasonic wave propagation predictions for polycrystalline materials using three dimensional synthetic microstructures: attenuation, J. Acoust. Soc. Am. 145 (4) (2019) 2181–2191.
[22] R.K. Roney, The Influence of Metal Grain Size on the Attenuation of an Ultrasonic Wave (Ph.D. Disseration), California Institute of Technology, 1950.
[23] R. Smith, The effect of grain size distribution on the frequency dependence of the ultrasonic attenuation in polycrystalline materials, Ultrasonics 20 (5) (1982) 211–214.
[24] D. Nicoletti, A. Anderson, Determination of grain-size distribution from ultrasonic attenuation: transformation and inversion, J. Acoust. Soc. Am. 101 (2) (1997) 686–689.
[25] A. Arguelles, J.A. Turner, Ultrasonic attenuation of polycrystalline materials with a distribution of grain sizes, J. Acoust. Soc. Am. 141 (6) (2017) 4347–4353.
[26] X. Bai, Y. Zhao, J. Ma, Y. Liu, Q. Wang, Grain-size distribution effects on the attenuation of laser-generated ultrasound in α-titanium alloy, Materials 12 (1) (2019) 102.
[27] G. Sha, Correlation of elastic wave attenuation and scattering with volumetric grain size distribution for polycrystals of statistically equiaxed grains, Wave Motion 83 (2018) 102–110.
[28] M. Ryzy, T. Grabec, P. Sedlák, I.A. Veres, Influence of grain morphology on ultrasonic wave attenuation in polycrystalline media with statistically equiaxed grains, J. Acoust. Soc. Am. 143 (1) (2018) 219–229.
[29] M.A. Groeber, M.A. Jackson, DREAM.3D: a digital representation environment for the analysis of microstructure in 3D, Integrating Mater. Manuf. Innov. 3 (1) (2014) 5.
[30] A.G. Every, A.K. McCurdy, "Second and higher-order elastic constants, Landolt-Börnstein Numerical Data and Functional Relationships in Science and Technology New Series Group III: Crystal and Solid State Physics, vol. 29a, Springer-Verlag, Berlin, 1992.
[31] M. Ardeljan, R. McCabe, I. Beyerlein, M. Knezevic, Explicit incorporation of deformation twins into crystal plasticity finite element models, Comput. Methods Appl. Mech. Eng. 295 (Supplement C) (2015) 396–413.
[32] M. Knezevic, B. Drach, M. Ardeljan, I. Beyerlein, Three dimensional predictions of grain scale plasticity and grain boundaries using crystal plasticity finite element models, Comput. Methods Appl. Mech. Eng. 277 (2014) 239–259.
[33] M. Norouzian, J.A. Turner, Ultrasonic wave propagation predictions for polycrystalline materials using three-dimensional synthetic microstructures: Phase velocity variations, J. Acoust. Soc. Am. 145 (4) (2019) 2171–2180.
[34] G. Ghoshal, J.A. Turner, Diffuse ultrasonic backscatter at normal incidence through a curved interface, J. Acoust. Soc. Am. 128 (6) (2010) 3449–3458.
[35] X. Li, Y. Song, A.P. Arguelles, J.A. Turner, Diffuse ultrasonic backscatter using a multi-gaussian beam model, J. Acoust. Soc. Am. 142 (1) (2017) 195–205.
[36] C.M. Kube, Iterative solution to bulk wave propagation in polycrystalline materials, J. Acoust. Soc. Am. 141 (3) (2017) 1804–1811.
[37] P. Hu, J.A. Turner, Transverse-to-transverse diffuse ultrasonic scattering, J. Acoust. Soc. Am. 142 (2) (2017) 1112–1120.
[38] Y. Song, J.A. Turner, Z. Peng, C. Chen, X. Li, Enhanced ultrasonic flaw detection using an ultrahigh gain and time-dependent threshold, IEEE Trans. Ultrasonics Ferroelectr. Frequency Control 65 (7) (2018) 1214–1225.
[39] E.P. Papadakis, Rayleigh and stochastic scattering of ultrasonic waves in steel, J. Appl. Phys. 34 (2) (1963) 265–269.
[40] D. Nicoletti, N. Bilgutay, B. Onaral, Power-law relationships between the dependence of ultrasonic attenuation on wavelength and the grain size distribution, J. Acoust. Soc. Am. 91 (6) (1992) 3278–3284.
[41] S. Sarkar, A. Moreau, M. Militzer, W.J. Poole, Power-law relationships between the dependence of ultrasonic attenuation on wavelength and the grain size distribution, Metall. Mater. Trans. A 39 (4) (2008) 897–907.
[42] E.R. Generazio, Ultrasonic attenuation measurements determine onset, degree, and completion of recrystallization, Mater. Eval. 46 (1988) 1198–1203.
[43] M. Dubois, M. Militzer, A. Moreau, J.F. Bussière, A new technique for the quantitative real-time monitoring of austenite grain growth in steel, Scripta Mater. 42 (9) (2000) 867–874.
[44] T. Garcin, J.H. Schmitt, M. Militzer, In-situ laser ultrasonic grain size measurement in superalloy INCONEL 718, J. Alloy. Compd. 670 (9) (2016) 329–336.